scientific reports

Check for updates

OPEN

The metalloproteinase PAPP-A is required for IGF-dependent chondrocyte differentiation and organization

Mette Harboe[1], Kasper Kjaer-Sorensen[1], Ernst-Martin Füchtbauer[1], Robert A. Fenton[2], Jesper Skovhus Thomsen[2], Annemarie Brüel[2] & Claus Oxvig[1]✉

Insulin-like growth factor (IGF) signaling is required for proper growth and skeletal development in vertebrates. Consequently, its dysregulation may lead to abnormalities of growth or skeletal structures. IGF is involved in the regulation of cell proliferation and differentiation of chondrocytes. However, the availability of bioactive IGF may be controlled by antagonizing IGF binding proteins (IGFBPs) in the circulation and tissues. As the metalloproteinase PAPP-A specifically cleaves members of the IGFBP family, we hypothesized that PAPP-A activity liberates bioactive IGF in cartilage. In PAPP-A knockout mice, the femur length was reduced and the mice showed a disorganized columnar organization of growth plate chondrocytes. Similarly, zebrafish lacking *pappaa* showed reduced length of Meckel's cartilage and disorganized chondrocytes, reminiscent of the mouse knockout phenotype. Expression of chondrocyte differentiation markers (*sox9a*, *ihha*, and *col10a1*) was markedly affected in Meckel's cartilage of *pappaa* knockout zebrafish, indicating that differentiation of chondrocytes was compromised. Additionally, the zebrafish *pappaa* knockout phenotype was mimicked by pharmacological inhibition of IGF signaling, and it could be rescued by treatment with exogenous recombinant IGF-I. In conclusion, our data suggests that IGF activity in the growing cartilage, and hence IGF signaling in chondrocytes, requires the presence of PAPP-A. The absence of PAPP-A causes aberrant chondrocyte organization and compromised growth in both mice and zebrafish.

Keywords Insulin-like growth factor, Growth plate, Chondrocyte, Proteolytic regulation, Animal models

Abbreviations

PAPP-A	Pregnancy-associated plasma protein-A
IGF	Insulin-like growth factor
IGFBP	IGF binding protein

Bone elongation is regulated by local and systemic growth factors, including those of the growth hormone (GH)/insulin-like growth factor (IGF) axis. The classical principle is that pituitary GH causes hepatic secretion of IGF-I into the circulation, but local actions of GH and local synthesis of IGF-I are important in many tissues, including bone[1,2].

In mammals, longitudinal bone growth occurs at the site of the epiphyseal growth plate. It involves chondrocytes going through a series of stages, each reflected by histologically distinct zones: The germinal zone (GZ), the proliferative zone (PZ), and the hypertrophic zone (HZ). The GZ contains small, rounded, quiescent chondrocytes. The PZ is composed of chondrocytes in a characteristic and highly organized columnar arrangement. At the base of the chondrocyte columns, the PZ transforms into the HZ, where chondrocytes become terminally differentiated and exit the cell cycle[3]. A continuous supply of chondrocytes in the direction from the GZ to the HZ, and the increase in height/size of the hypertrophic chondrocytes is important in order to maintain an active growth plate and thus balanced extension of the growing bone[1,4].

Both IGF-I and its receptor (IGF-IR) are expressed by growth plate chondrocytes[3,5], and IGF-I promotes both chondrocyte proliferation and differentiation and thereby induce growth plate elongation[6]. However, in addition to spatially regulated synthesis, additional layers regulating IGF bioactivity in the extracellular compartment

[1]Department of Molecular Biology and Genetics, Aarhus University, Universitetsbyen 81, 8000 Aarhus C, Denmark. [2]Department of Biomedicine, Aarhus University, Aarhus, Denmark. ✉email: co@mbg.au.dk

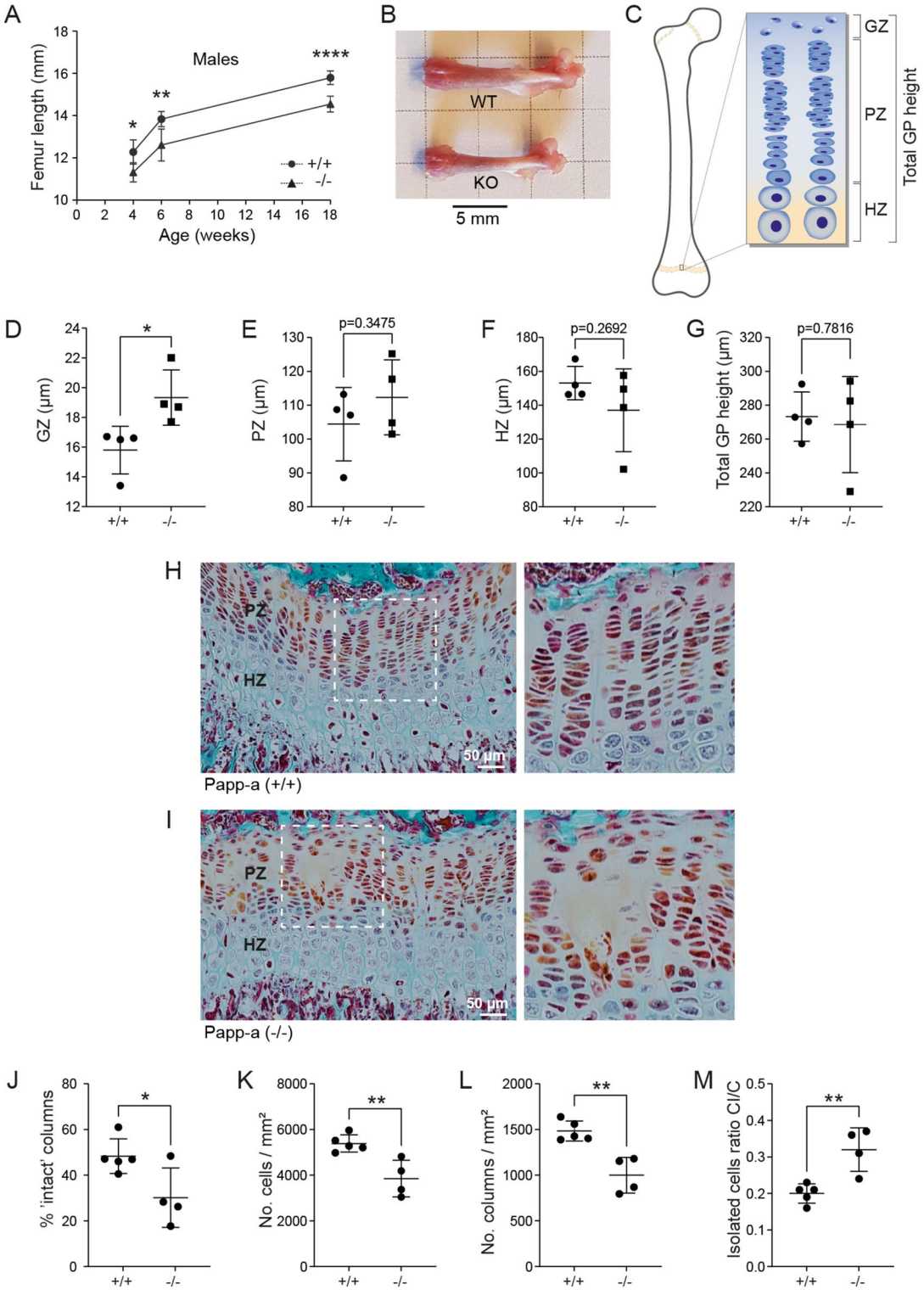

have been proposed. Free IGF-I is antagonized by high-affinity binding to one of six IGF binding proteins (IGFBP-1–6), thus regulating the level of bioavailable IGF-I in the pericellular environment[7]. From these IGF-IGFBP complexes, bioactive IGF can be released by proteolytic cleavage of the IGFBP in its central part, widely described in vitro[7]. The pappalysin metalloproteinase pregnancy-associated plasma protein-A (PAPP-A)[2,8–11] has enzymatic activity specifically towards IGFBP-2[12], -4[13], and -5[14] with no other substrates known, and thus is tightly connected to the regulation of IGF signaling. Disruption of the murine *Pappa* gene results in a postnatal reduction in body weight of approximately 40%, and compromised bone microarchitecture[15,16], indicating that PAPP-A exerts an anabolic effect on size-related bone parameters by increasing IGF bioavailability.

Thus, although IGF historically is known to be a key player in bone growth, any local regulatory effect of PAPP-A, i.e. at the level of the growth plate and thereby in bone elongation, remains unexplored. To address

◂**Fig. 1.** PAPP-A knockout in mice causes reduced bone length and growth plate chondrocyte disorganization. (**A**) Femoral bone length in male wild-type and knockout mice at postnatal week 4, 6 and 18. The number of mice (wild-types/knockouts males): 4 weeks, (5/5); 6 weeks (6/6); 18 weeks, (10/5). (**B**) Representative examples of intact femurs from wild-type or knockout PAPP-A mice at 6 weeks of age. (**C**) Schematic drawing indicating the positions of the growth plate germinal zone (GZ), the proliferative zone (PZ), the hypertrophic zone (HZ), and the total growth plate (GP) height. (**D**–**G**) Heights of the GZ (**D**), the PZ (**E**), the HZ (**F**), and the total growth plate height (**G**) was measured on growth plate sections stained with Masson–Goldner trichrome from 4 weeks old male Pappa wild-type (+/+) and knockout (−/−) mice. The data are based on 4 wild-type and 4 knockout mice. (**H**–**I**) Representative examples of growth plates sections from 4 weeks old male *Pappa* wild-type (+/+) and knockout (−/−) mice, respectively. The boxed areas of the proliferative zone are shown at a higher magnification to the right. Note that the proliferative zone of the PAPP-A knockout shows areas devoid of chondrocytes. (**J**–**M**) Quantification of growth plate columnar organization using grid-based analysis[31]. The data are based on 5 wild-type and 4 knockout mice. (**J**) The percentage of intact columns, i.e. columns with chondrocytes continuously across the full height of the proliferative zone. (**K**) Cell density in the proliferative zone. (**L**) Column density in the proliferative zone. (**M**) Isolated cells ratio (CI/C), reported as the proportion of isolated cells (CI) per grid field among the total cell number (C) within a grid field (increased by 60% in Pappa knockout compared to wild-type mice). This parameter describes the quality of columnar arrangement, with a high CI/C ratio indicating a high proportion of chondrocytes not organized into columns[31]. Data are mean ± SD and are analyzed by unpaired two-tailed Student's t-test. ns, $p > 0.05$; * $p < 0.05$; ** $p < 0.01$; *** $p < 0.001$; **** $p < 0.0001$.

this, we first compared bone length and epiphyseal growth plates of wild-type and PAPP-A knockout mice. For further morphological and molecular analyses, we used cartilage elements of genetically modified zebrafish.

Results

Reduced bone length and growth plate chondrocyte disorganization in PAPP-A knockout mice

In order to study bone growth in the absence of PAPP-A, we generated a knockout mouse model by using CRISPR/Cas9 technology and assessed longitudinal growth. At weeks 4, 6 and 18 of age, male PAPP-A knockout mice showed a significant reduction (ca. 7%, $p = 0.03$) in femur length compared to wild-type mice. The absolute differences in femur length were not further increased after week 6 (Fig. 1A,B). At 4 weeks of age, the body mass of knockout mice (11.7 g ± 1.18) was significantly ($p = 0.001$) reduced compared to wild-type mice (18.4 g ± 2.34), in agreement with the earlier published PAPP-A knockout model[15]. Similar data was obtained for female mice (not shown).

To understand the cause of this longitudinal growth retardation at the cellular level, growth plate morphology was assessed by histological analyses of the growth plate at the distal femoral metaphysis at week 4 in male mice (Fig. 1C–G). The total height of the growth plate (wild-type mice: 273.2 µm ± 14.6; knockout mice: 268.6 µm ± 28.4), GZ height (wild-type mice: 15.8 µm ± 1.6; knockout mice: 19.3 µm ± 1.9), PZ height (wild-type mice: 104.4 µm ± 10.8; knockout mice: 112.3 µm ± 11.1), and the HZ height (wild-type mice: 153 µm ± 9.9; knockout mice: 137.0 µm ± 24.5) were determined. Thus, in PAPP-A knockout mice, the height of the GZ was significantly increased ($p = 0.028$) in knockout mice.

Interestingly, in PAPP-A knockout mice the PZ exhibited large areas devoid of chondrocytes (Fig. 1H–I) and the percentage of intact columns of chondrocytes was significantly decreased (Fig. 1J). Analysis of the chondrocytes within this zone revealed a significantly reduced cell density and column density in the PAPP-A knockout mice (Fig. 1K–L). Moreover, an increased isolated cell ratio demonstrated that a high proportion of the chondrocytes were not organized into columns (Fig. 1M). In summary, ablation of PAPP-A reduces the longitudinal growth of the murine femur and results in disruptions of the columnar organization of chondrocytes in the PZ.

Normal craniofacial cartilage development in zebrafish requires PAPP-A

To further investigate the regulatory role of PAPP-A in cartilage growth at the cellular level, we utilized the zebrafish model, which provides key experimental advantages compared to the murine model. Zebrafish craniofacial cartilage has been used to model cartilage dynamics due to its less complex cellular organization compared to the growth plate of mammals. Importantly, the cellular mechanisms and fundamental signaling pathways involved in chondrogenesis are conserved between mammals and zebrafish[17,18]. The zebrafish genome carries two orthologues of the PAPP-A gene (*pappaa* and *pappab*)[19], and a single orthologue of the homologous PAPP-A2 gene (*pappa2*), which we also included in the analysis. For all of the pappalysins in any species studied, proteolytic substrates other than IGFBPs have not been identified. Biochemical analyses of the human, mouse, and zebrafish pappalysins, demonstrating abilities to specifically cleave IGFBPs and thus release bound IGF, have been carried out earlier[14,19–22].

At 4 days post fertilization (dpf), all craniofacial structures, which are composed of cartilage, have been formed in the zebrafish larvae (Fig. 2A)[23]. Alcian blue staining was performed on 4 dpf knockout (−/−) and wild-type (+/+) larvae obtained from heterozygous crosses of *pappaa* (*pappaa(Sa17987)*) (−/+), *pappab* (*pappab(Auzf1)*) (−/+), and *pappa2* (*pappa2(Sa17244)*) (−/+) lines. The overall morphology of the craniofacial cartilage elements was preserved in knockout larvae of all three lines (Fig. 2B–G). However, in *pappaa* knockout larvae the rod-shaped cartilage elements were less slender and more irregular in shape compared to wild-type larvae (Fig. 2B–C). Also, the bilateral Meckel's cartilage (Fig. 2A), which gives rise to the anterior part of the lower jaw, was significantly shorter in pappaa knockouts compared to wild-type siblings (Fig. 2H). Elongation of Meckel's cartilage depends on coordinated cell–cell intercalations, during which the chondrocytes become

Fig. 2. Zebrafish devoid of Papp-aa display reduced size of Meckel's cartilage and aberrant chondrocyte morphology. (A) Lateral and ventral views of wild-type zebrafish (4 dpf) stained with Alcian blue. Schematic overview of the pharyngeal cartilage elements of the zebrafish viscerocranium is shown. As indicated, the length of Meckel's cartilage (m) was measured from its anterior edge to the posterior edge, which articulates with the palatoquadrate (p). (**B**–**G**) Representative ventral images of *pappaa, pappab,* and *pappa2 knockout* (−/−) and wild-type (+/+) heads, as indicated, stained with Alcian blue. Magnifications of Meckel's cartilage (boxed area in B), corresponding to the larvae shown in B-G and derived outlines of the chondrocytes are also shown. (**H**–**J**) The length of Meckel's cartilage, measured as shown in A, for wild-type (n = 20) and knockout (n = 20) *pappaa*, wild-type (n = 13) and knockout (n = 9) *pappab,* and wild-type (n = 16) and knockout (n = 17) *pappa2*, respectively. (**K**) Expression of *pappaa* detected by whole mount in situ hybridization using a gene specific probe. Arrowhead mark expression in Meckel's cartilage. (**L**–**N**) Chondrocyte morphology assessed in the transgenic zebrafish line *pappaa(Sa17987);Tg(fli1a:eGFP)*, which expresses GFP in the craniofacial cartilage. (**L**) Representative confocal images of one side of Meckel's cartilage in wild-type and knockout larvae. (**M**) Chondrocyte length/width ratio within the middle third of Meckel's cartilage. (**N**) The number of neighboring cells of each chondrocyte within the middle third of Meckel's cartilage (**K**). *pappaa* data are from three, *pappab* data are from two, and *pappa2* data are from four independent experiments. (**N**) The number of neighboring cells of each chondrocyte (**K**). *pappaa* data are from three, and *pappab* data are from two independent experiments. The results are shown as mean ± SD and analyzed by unpaired two-tailed Student's t-test. * $p < 0.05$; ** $p < 0.01$.

ellipsoid and arrange into highly regular stacks[24], as evident in the wild-type fish. In *pappaa* knockout larvae, the chondrocytes of Meckel's cartilage appeared disorganized and less uniformly shaped compared to wild-types (Fig. 2B–C), thus recapitulating the disorganized chondrocyte phenotype observed in PAPP-A knockout mice. Whole-mount in situ hybridization (WISH) showed the expression of *pappaa* mRNA in Meckel's cartilage at 4 dpf (Fig. 2K). In both *pappab* and *pappa2* knockout larvae, chondrocyte shape and organization, as well as the length of Meckel's cartilage, were not significantly affected (Fig. 2D–G,I–J). In summary, these experiments suggest that of the three pappalysins, *pappaa* is the most important for IGF regulation in the cartilage element of our focus and is expressed locally in this tissue.

To quantitatively assess the effect of *pappaaa* knockout on chondrocyte morphology, transgenic *pappaa(Sa1978);Tg(fli1a:eGFP)* zebrafish were generated. Larvae from this line show a strong fluorescent signal in chondrocytes of the developing cartilage elements[25], allowing Meckel's cartilage to be imaged in detail by confocal microscopy. By visual inspection, the disorganization of chondrocytes is evident in the absence of Papp-aa, and unlike in wild-type siblings, chondrocytes did not span the mediolateral width of the element (Fig. 2L). The length/width ratio of the individual chondrocytes in the middle third of Meckel's cartilage was quantified. Compared to wild-type siblings, this was significantly reduced in *pappaa* knockout larvae (Fig. 2M). Furthermore, the average number of neighboring cells of individual chondrocytes, was significantly increased (Fig. 2N). In summary, Papp-aa is required for proper organization and morphology of the chondrocytes in Meckel's cartilage, and likely has a role in this tissue, similar to the role of PAPP-A in the murine growth plate.

Marker gene expression show impaired chondrocyte differentiation in *pappaa* knockout larvae

Chondrocyte differentiation is characterized by a dramatic change in cell shape and size. Based on the changed morphology of the chondrocytes in Meckel's cartilage, we reasoned that the absence of Papp-aa might affect chondrocyte differentiation. We therefore assessed the expression of selected chondrogenesis marker genes by WISH at 4 dpf (Fig. 3): The SRY-box transcription factor 9 (*sox9a)* is an essential regulator of the chondrocyte lineage[26]. It was expressed in all craniofacial cartilage elements, including Meckel's cartilage at 4 dpf (Fig. 3A–B), and there was no significant differences between *pappaa* wild-type and knockout larvae (Fig. 3A,B,G). The transcription factor Indian hedgehog a (*ihha*) is expressed by prehypertrophic chondrocytes[27]. Sparse expression of *ihha* in Meckel's cartilage at this developmental stage did not allow reliable quantification, but by visual inspection, it was evident that *ihha* expression was reduced to an almost undetectable level in the *pappaa* knockout larvae (Fig. 3C–D). Quantification of the expression of *ihha* in a neighboring cartilage element showed a significant reduction (Fig. 3H). Lastly, expression of collagen type 10a1a (*col10a1a*), also expressed by perichondral cells and osteoblasts, indicates a mature stage of hypertrophic chondrocytes[27,28]. We observed pronounced staining ventral to Meckel's cartilage (Fig. 3E–F), which was significantly reduced in the *pappaa* knockout larvae (Fig. 3E–F,I). In growth plates of PAPP-A knockout mice, we did not observe any differences in Ihh expression (data not shown), but we verified a corresponding difference in expression of ColX in the mouse growth plate hypertrophic zone, but not in the combined germinal and proliferative zones (Fig. 3J).

Papp-aa regulation of cartilage development depends on IGF signaling

By means of its proteolytic activity towards IGFBPs, PAPP-A potentially increases IGF bioactivity and hence IGF signaling[8]. To establish whether Papp-aa modulates cartilage development through IGF signaling, we assessed the effect of pharmacological inhibition of IGF signaling on cartilage formation. Exposure of wild-type zebrafish to the IGF-IR inhibitor NVP-AEW541[29], and the structurally different inhibitor, BMS-754807[30], resulted in both aberrant chondrocyte organization (Fig. 4A–B,D–E) and shortening of Meckel's cartilage (Fig. 4), similar to the *pappaa* knockout phenotype (Fig. 2).

To substantiate that the cartilage phenotype of the *pappaa* knockout larvae is caused by compromised IGF signaling, we attempted to rescue the phenotype by exposing the larvae to exogenous IGF-I. Thus, larvae were treated with IGF-I during the period from 3 to 4 dpf and stained with Alcian blue. We found that IGF-I treatment

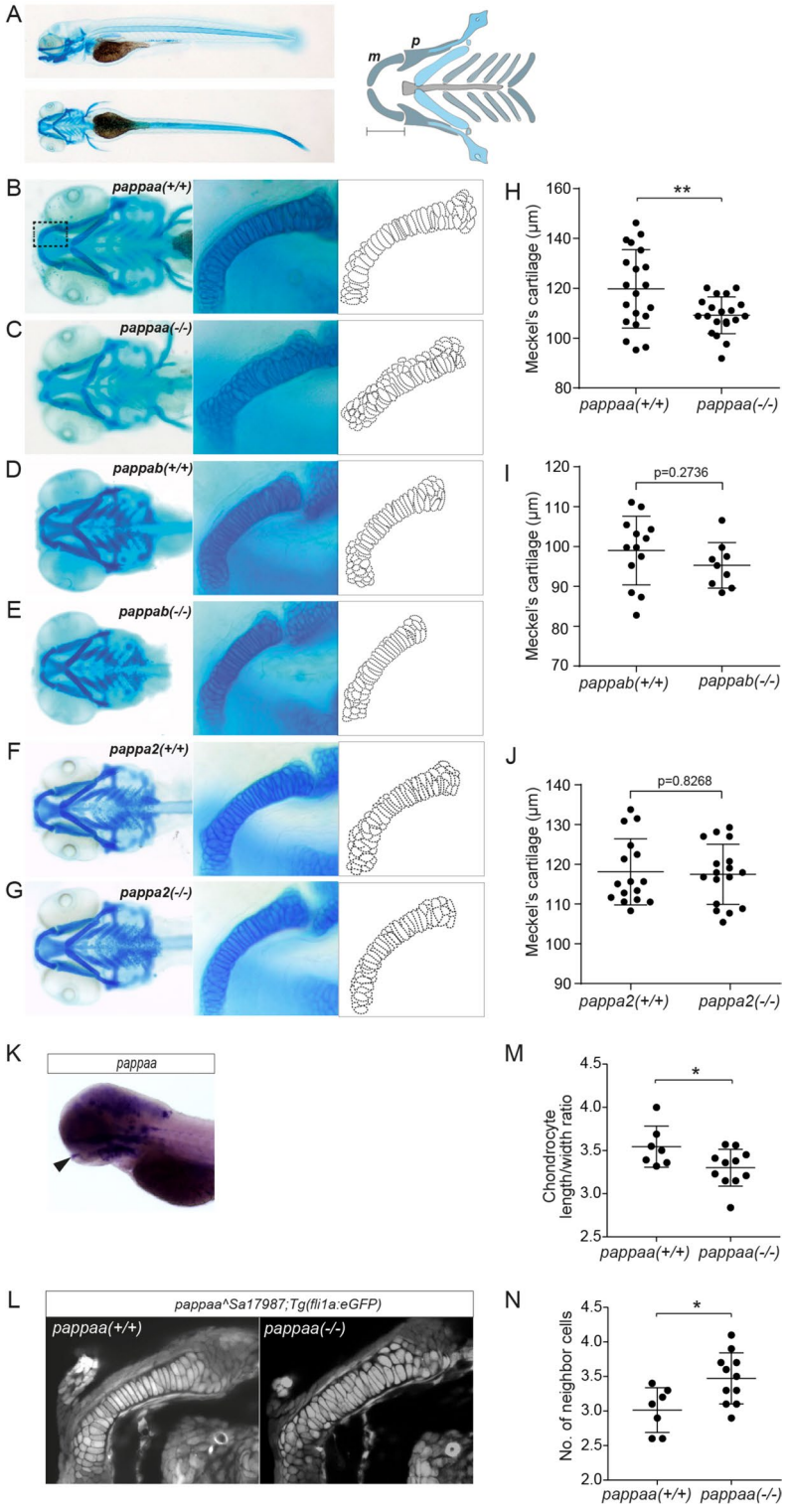

rescued the disorganized appearance of chondrocytes of the *pappaa* knockout (Fig. 5A–C) as well as the length of Meckel's cartilage (Fig. 5D). In addition, treatment of *pappaa* knockout larvae with IGF-I significantly normalized the expression of *col10a1a* compared to untreated *pappaa* knockout larvae (Fig. 5E–F).

Discussion

We have analyzed longitudinal growth and chondrocyte differentiation in the absence of the metalloproteinase, PAPP-A in mice and zebrafish. The absence of PAPP-A reduced femur length in male and female mice, and caused a significant increase in growth plate germinal zone height. The height of the proliferative zone (PZ) was not significantly altered, but rather than ordered columns of chondrocytes, the PZ exhibited large areas devoid of chondrocytes, and a reduced number of intact columns making contact to both the germinal zone and the

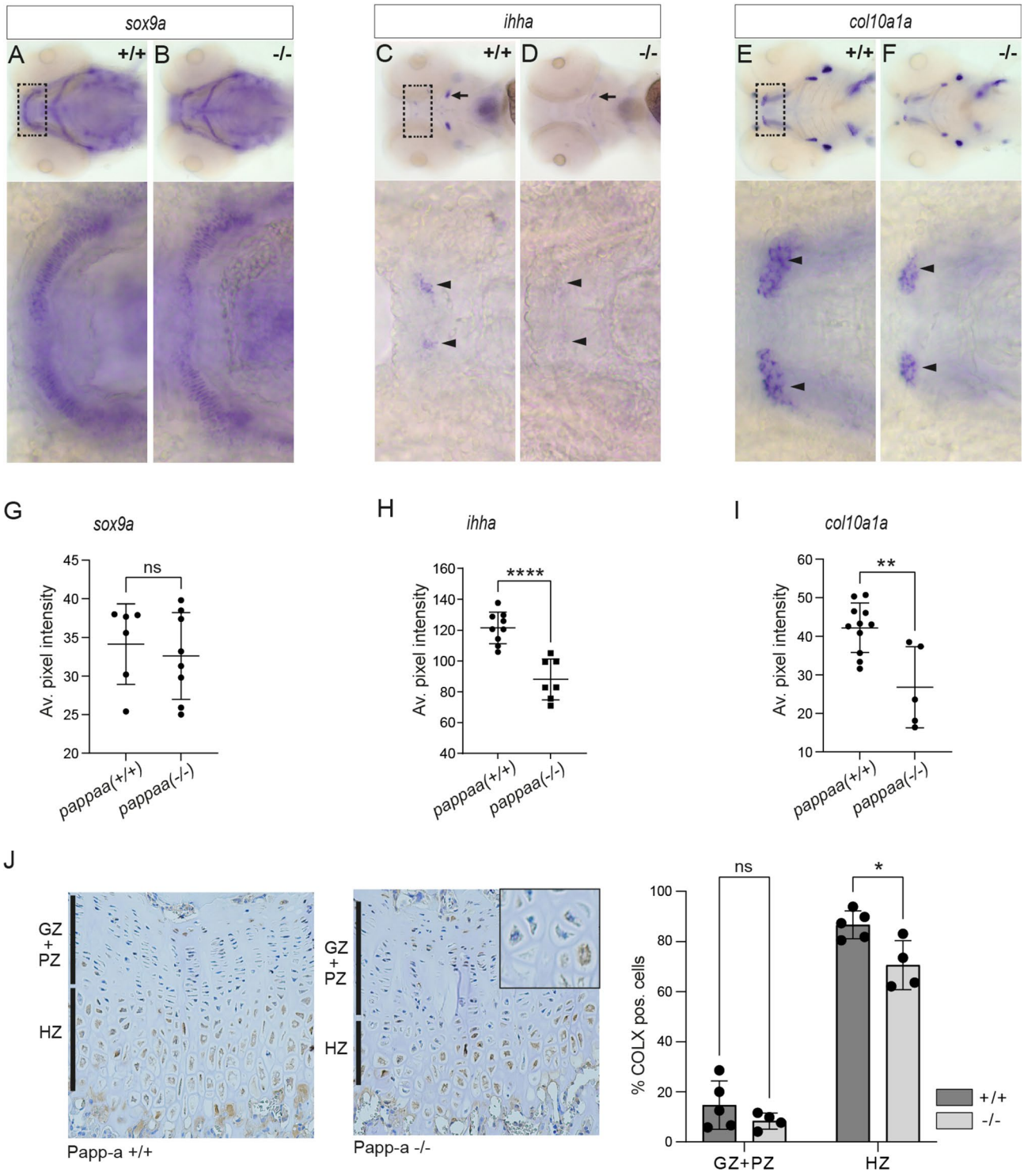

Fig. 3. Altered expression of chondrocyte differentiation markers *sox9a*, *col10a1a* and *ihha* in *pappaa* knockout larvae. At 4 dpf, the expression of *sox9a, ihha*, and *col10a1* was assessed in wild-type and *pappaa* knockout larvae by whole mount in situ hybridization. (**A**,**B**) Expression of *sox9a*, a transcription factor expressed during early chondrogenesis essential for initiating and maintaining chondrogenesis[26]. (**C**,**D**) Expression of *ihha*, a paracrine factor synthesized by prehypertrophic chondrocytes[27]. Staining of *ihha* in the ceratohyal (arrows) or Meckel's (arrowheads) cartilage is indicated. (**E**,**F**) Expression of *col10a1a*, an ECM component synthesized by hypertrophic chondrocytes[27]. In zebrafish, perichondral expression has also been reported around Meckel's cartilage (arrowheads)[28]. (**G**–**I**) Average intensity of the staining in Meckel's/ceratohyal cartilage for *sox9a, ihha,* and *col10a1a*, respectively. (**J**) Immunostaining of growth plate sections from wild-type or PAPP-A knockout mice, as indicated (left panels) using an antibody specific for mouse COLX. Quantification of the number of COLX-positive chondrocytes is shown for the germinal and proliferative zones combined (GZ + PZ) and for the hypertrophic zone (HZ) (right panel). An example of COLX-negative and -positive hypertrophic chondrocytes in the growth plate of PAPP-A knockout mouse is shown (inset).

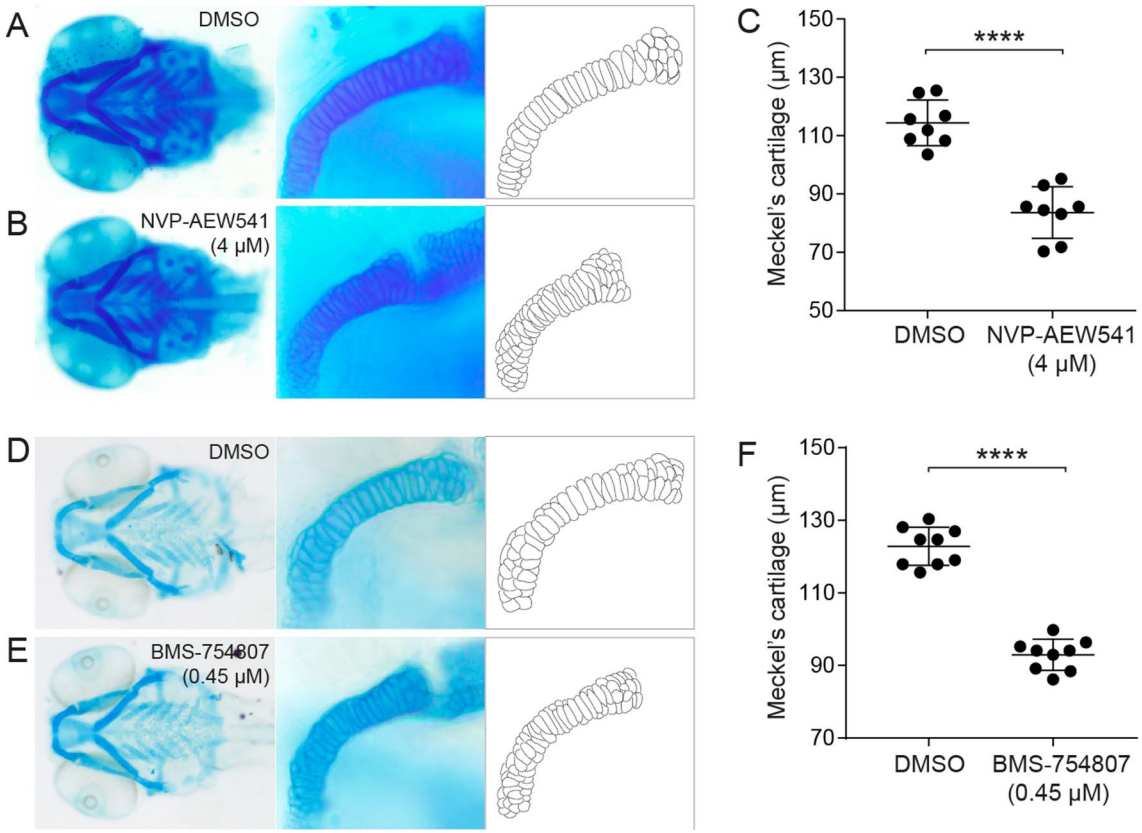

Fig. 4. Normal morphology of Meckel's cartilage depends on IGF signaling. (**A**,**B**) Representative images of Alcian blue-stained wild-type zebrafish larvae treated with the IGF-IR inhibitor NVP-AEW541 (4 μM) or control solution (DMSO in E3) from 3 to 4 dpf. A magnification of one side of Meckel's cartilage and a schematic outline of the chondrocytes in Meckel's cartilage are also shown. (**C**) Length of Meckel's cartilage after control (n = 8) and NVP-AEW541 (n = 8) treatment. Data are from two independent experiments. (**D**–**F**) A similar experiment using the structurally distinct IGF-IR inhibitor BMS-75807 (0.45 μM, n = 9; control group, n = 9). Data are from three independent experiments. Results are shown as mean ± SD, and are analyzed by Student's t-test. ****$p < 0.0001$.

hypertrophic zone. The isolated cells ratio (CI/C[31]), was increased by 60%, showing that a significantly higher proportion of the chondrocytes were not organized into columns in the knockout mice. Interestingly, a similarly disorganized columnar structure of the PZ has been observed in mice with tamoxifen-inducible cartilage-specific knockout of the IGF-IR[32]. Together, these data are in agreement with an important role of PAPP-A in local regulation of IGF signaling in the cartilage.

In order to further study PAPP-A in vertebrate chondrocyte development, we assessed the craniofacial cartilage of zebrafish in the absence of the two PAPP-A paralogues, *pappaa* and *pappab*, and the single PAPP-A2 paralogue, *pappa2*, all of which are present in zebrafish. For the *pappab* and *pappa2* knockouts, no cartilage phenotype was observed. For the *pappaa* knockout, the craniofacial cartilage elements were distorted, and the length of Meckel's cartilage was significantly reduced. Additionally, *pappaa* knockouts showed characteristic and significant alterations of chondrocyte organization in Meckel's cartilage, including a reduction in the chondrocyte length/width ratio and an increase in the neighboring cell number. Thus, the cartilage phenotype of zebrafish lacking Papp-aa is reminiscent of the phenotype observed in PAPP-A knockout mice. By whole mount in situ hybridization, we demonstrated decreased expression of *ihha* and *col10a1a* in *pappaa* knockouts, suggesting that terminal differentiation of chondrocytes is compromised in the absence of Papp-aa. Ihh is similarly dysregulated in IGF-IR deficient mice[32], and COLX less abundant in IGFI deficient mice[33], suggesting that in cartilage, the absence of PAPP-A affects chondrocyte differentiation and thus cartilage integrity by regulating IGF.

In agreement with this, we further established that pharmacological inhibition of IGF signaling causes both a significant shortening of Meckel's cartilage, and a disturbed chondrocyte organization, thus mimicking the *pappaa* knockout phenotype, and supporting that it is caused by interrupted IGF signaling. We demonstrated this independently by using two mechanistically different synthetic inhibitors of IGF-IR signaling. Finally, to further connect the observed zebrafish Papp-a deficient phenotype with IGF signaling, we established that the *pappaa* knockout phenotype can be alleviated by treatment with recombinant IGF-I. Chondrocyte disorganization appeared to be fully rescued, and the length of Meckel's cartilage could not be distinguished as different from that of wild-type zebrafish. In addition, the treatment with IGF-I also restored the expression of *col10a1a*, a marker

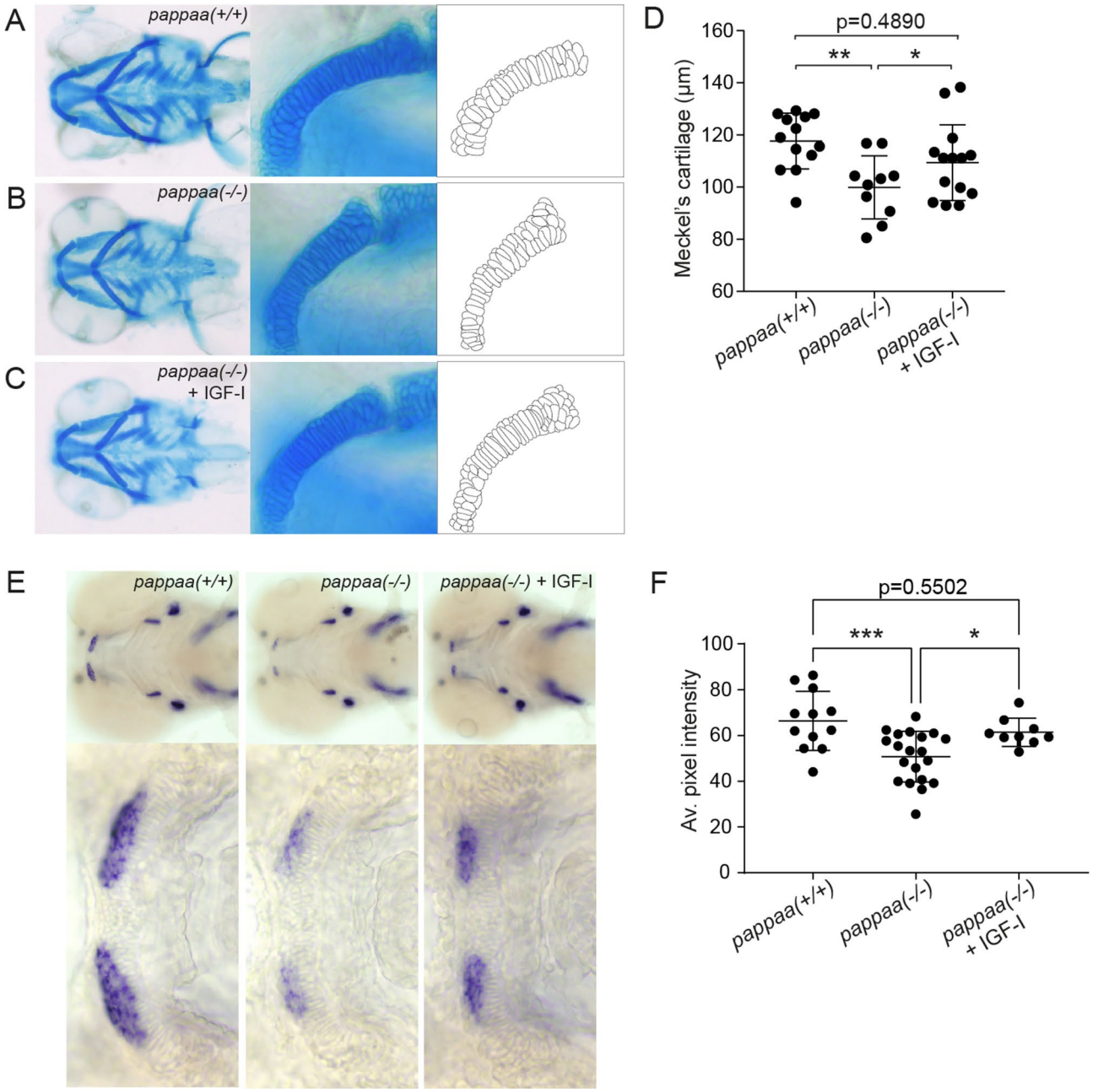

Fig. 5. Exogenous IGF-I restores normal morphology of Meckel's cartilage and expression of *col10a1a*. (**A**–**C**) 3 dpf *pappaa* knockout larvae were transferred to E3 buffer with or without 30 ng/mL IGF-I. At 4 dpf, the larvae were terminated, Alcian blue-stained and the length of Meckel's cartilage was determined. Representative ventral images of nontreated and IGF-I-treated larvae, corresponding magnifications of Meckel's cartilage, and outlines of the chondrocytes are shown. (**D**) Length of Meckel's cartilage for non-treated wild-type (n = 13) or knockout (n = 10) *pappaa,* and IGF-I-treated knockout *pappaa* (n = 14). (**E**) *Pappaa* knockout larvae were treated as described in (**A**), and stained for *col10a1a* by whole mount in situ hybridization. Representative ventral images and magnifications of Meckel's cartilage for are shown. (**F**) Average intensity of the *col10a1a* staining in Meckel's cartilage. Data are from three independent experiments, shown as mean ± SD and analyzed by one-way ANOVA. * $p < 0.05$; ** $p < 0.01$; *** $p < 0.001$; **** $p < 0.0001$.

of chondrocyte hypertrophy, supporting that Papp-aa plays an important role in proper cartilage development and terminal chondrocyte differentiation, and that this is mediated through IGF signaling.

PAPP-A is one of two proteinases of the pappalysin family. The other family member is the homologous PAPP-A2, which also exclusively cleaves IGFBP substrates (IGFBP-3 and -5). Thus, together PAPP-A and PAPP-A2 have the potential to release free, bioactive IGF from complexes with IGFBP-2, -3, -4, or -5[8]. Humans deficient in PAPP-A2 present with short stature, increased total IGF-I (present in IGFBP complexes), and decreased free IGF-I[34]. Human deficiency in PAPP-A has not been reported, but in contrast to PAPP-A2 deficiency, the

growth-retarded PAPP-A knockout mice do not have altered levels of circulating IGF-I[15]. Other data indirectly indicate that PAPP-A2 operates principally in the circulation, and that PAPP-A operates in tissues[2]. Thus, only PAPP-A exhibits cell surface tethering by its ability to bind surface glycosaminoglycan, facilitating release of bioactive IGF in close proximity to the IGF-IR[35,36]. However, the principle of PAPP-A and PAPP-A2 as local vs. systemic, respectively, is not without exceptions[2,37].

Studies have shown that a dramatic (75%) reduction in circulating IGF-I in mice by disrupted hepatic synthesis does not affect linear growth significantly[38,39], thus pointing at the importance of local synthesis and/or regulation[1,2,40]. However, proteolytic cleavage of IGFBPs is only variably considered as a possible mechanism of local regulation[3,41]. It was recently found that IGF signaling in Meckel's cartilage depends on locally synthesized IGF-I, and that deficient IGF signaling underlies mandibular hypoplasia in mice, and it was further speculated that IGF-I bioactivity is modulated by IGFBPs[42]. Importantly, previous data have shown that all known PAPP-A proteolytic substrates (IGFBP-2, -4 and -5) are indeed expressed in epiphyseal growth plate cartilage[43,44]. The present study shows that PAPP-A has a key role in normal growth plate function, thus specifically connecting PAPP-A with IGF function in this tissue. The absence of PAPP-A causes aberrant chondrocyte differentiation and compromised growth in both mice and zebrafish.

We show here that PAPP-A promotes normal growth plate function, but inhibition of PAPP-A proteolytic activity is also a regulatory mechanism potentially relevant to linear growth physiologically. Stanniocalcin-2 (STC2) was recently discovered as a potent inhibitor of PAPP-A[40]. By formation of a covalent 2:2 complex with PAPP-A[10], STC2 has the potential to determine the balance between active, IGF-promoting PAPP-A and inactive PAPP-A. Recent genetic analysis illustrates the relevance of this mechanism in vivo: Several single-residue variants of STC2, which show slightly compromised ability to inhibit PAPP-A, increase human height up to 2.1 cm[45].

Although a detailed analysis of the murine growth plate is beyond the scope of this study, we did verify a significant reduction of COLX-positive cells in the growth plate hypertrophic zone of knockout mice compared to wild-type mice. Our study thus justifies a thorough analysis of the dynamics of PAPP-A regulation in this more complicated tissue. Such analyses should involve analysis of classical marker genes, analysis of PAPP-A cell surface dynamics[35,36], as well as interactions with STC2 and other potential proteolytic inhibitors of PAPP-A[40,46,47]. Furthermore, recent genetic data point at human PAPP-A as a novel candidate effector gene causally involved in the development of osteoarthritis[48].

In summary, we have provided data showing that PAPP-A is important for proper bone elongation at the chondrocyte level in mice, and we have established the zebrafish as a suitable model for molecular analyses of this system. Data are emerging in support of the involvement of other proteins related to IGF signaling in chondrocyte dynamics, e.g. the PAPP-A inhibitor STC2, and future studies are required to fully understand the operation of the entire stanniocalcin-PAPP-A-IGFBP-IGF axis[2] in this tissue.

Methods

Generation of Papp-a knockout mice

Papp-a gene knockout was generated using CRISPR/Cas9 technology. Ten guide RNA candidates targeting exon 2 were identified by in silico analysis using the online design tool, CRISPOR (http://crispor.tefor.net/crispor.py)[49]. Complementary oligonucleotides containing the gRNA target and *BpiI*/*BbsI* overhangs were ligated into *BpiI*/*BbsI*-digested pX459 V2.0 plasmids[50] (Addgene #62,988) and transfected into murine 129 ES cells[51] using Lipofectamine 2000 (ThermoFisher Scientific). Based on the efficiency of the gRNAs and the frequency of indels introducing frameshift, as determined by TIDE analysis[52], one guide RNA was chosen for generation of transgenic mice (Guide RNA sequence: 5′-GACCCATCCTCGATCACGTG-3′). The plasmids expressing this gRNA were transfected into 129 ES cells and allowed to form single colonies. A colony containing a mutation causing a frameshift and premature stop codon in exon 2 was identified by PCR and Sanger sequencing. The ES cell colony was expanded and injected into B6D2 F2 blastocysts[53], which were then transferred to foster mice. Chimeric male offspring was bred with C57Bl/6J females, generating agouti offspring (indicating germ-line transmission) of the manipulated 129 derived ES cells which were analyzed for the presence of the knockout mutation. These mice were subsequently interbred to generate *Papp-a(−/−)*, *Papp-a(+/−)* and *Papp-a(+/+)* littermates. Genotyping was performed by Sanger sequencing after standard PCR amplification of DNA from ear biopsies using KOD Hotstart DNA polymerase (Novagen) and 0.5 µM of each of the primers: Fw:5′-TTATGGTAATGG CCCAAGACAC-3′, Rv:5′-ACCTACTTGCTCAGCCGAAG-3′. Previous *Papp-a* null mice were generated by in-frame deletion of exon 4[15]. The current mutation changed nucleotide 802–809 (CACGTGAT → TATA) causing a frameshift and thus introduced a premature stop codon in exon 2 (*Papp-a*, *Mus musculus* NM_021362.1). This results in a mature polypeptide of 90 amino acid residues (A1-T65[22], followed by 25 residues, LYEDGSWAFTP-PVIKATEIHATFSP), thus terminated within in the laminin G-like domain and unlikely to fold into native-like protein[54]. Mice were kept on a 12h light/12h dark cycle with access to food pellets (Altromin 1324) and water ad libitum. All mouse work was conducted with the permission of the Danish Animals Ethics Council (permit number 2017-15-0202-00055). The work was based on mice from Janvier Labs, France. All experiments were carried out in accordance with relevant guidelines and regulations, and are reported in accordance with ARRIVE guidelines (https://arriveguidelines.org).

Bone length and growth plate histology

For bone collection, mice were euthanized by cervical dislocation at postnatal week 4 (pre-puberty), 6 (puberty), or 18 (adult). The femora were removed and fixed in 4% PFA for 48 h at 4 °C, and then stored in 70% ethanol at 4 °C until analysis. The femoral bone length was measured from the medial condyle to the top of the femoral head using a digital sliding caliper. The distal half of the mouse femora were embedded, decalcified in methyl methacrylate (MMA), frontal 7 µm-thick sections were cut using a microtome (Jung RM2065; Leica Instruments,

Nussloch, Germany), and sections were stained with Masson–Goldner trichrome. Light microscopy images of the murine growth plates were acquired using a Zeiss Axio Scope A1 microscope equipped with a Nikon D800 camera. Quantification of columnar organization in the PZ of murine growth plates was carried out according to the grid-based method[31]. One femur from each animal was used and two sections from each femur were analyzed. A grid with field sizes of 33 µm × 33 µm was applied to 20 × magnified images and a minimum of 30 grid fields per section were analyzed. Within each grid field of the proliferative zone, the cellular density (C) (i.e. the total number of cells, where 90% of the cell must be within the grid field), the column density (CD), and the density of isolated cells (CI) were determined. Results per grid field were averaged, and the total cell number and column density expressed as cells per area (mm2). Furthermore, the isolated cells ratio (CI/I) was determined as the number of isolated cells per total number of cells. All measurements were performed using ImageJ[55]. Similarly, frontal 2 µm-thick sections were stained with a polyclonal rabbit-anti-mouse COLX antibody (Abcam ab58632, dilution 1:4500). Secondary goat anti-rabbit HRP-conjugated antibody (DAKO P448, dilution 1:200) was used, and the sections were counterstained (Mayer's). Chondrocytes in the growth plate were analyzed at a total magnification of × 1020 using a Nikon Eclipse i80 microscope (Tokyo, Japan), projecting images to a computer with Visiopharm (v. 2020.09, Visiopharm, Hørsholm, Denmark) stereology software. Across a distance of 500 µm, the number of positively stained cells were counted in the GZ and PZ collectively and in the HZ.

Zebrafish maintenance and genotyping

Wild-type AB, *Tg(fli1a:eGFP)*[25], *pappaa(Sa17987)*[56], and *pappa2(Sa17244)*[56] lines were obtained from the European Zebrafish Resource Center, Karlsruhe, Germany). *pappabAuzf1*[57] was generated by us. All zebrafish were maintained at 28 °C in reverse osmosis water reconditioned to pH 7.2 and 700 µS with sodium bicarbonate and Instant Ocean Sea Salt (Aquarium System) with a 14–10-h light–dark cycle on recirculating housing systems. Embryos were obtained by natural crosses and raised at 28 °C in E3 buffer (5 mM NaCl, 0.17 mM KCl, 0.33 mM CaCl2, 0.33 mM MgSO4, 10 − 5 (w/w) methylene blue, 2 mM HEPES, pH 7.4). All experiments were carried out according to Danish legislation and approved by The Danish Animal Ethics Council (permit number 2017–15-0201–01,369). Euthanasia of zebrafish larvae was done with an overdose of tricaine. Samples for adult zebrafish genotyping were obtained by swabbing[58]. Samples for genotyping were taken from the embryos after euthanasia and fixed in MeOH for 15–30 min at RT followed by tissue digestion in TE buffer with 17 mg/mL Proteinase K (Ambion) for 2–4 h at 55 °C followed by enzyme inactivation 5 min at 95 °C. PCR was performed using the following primers: pappaa-f, 5′-ATCGTTGTCAATTTTCTGCAGCC-3′; pappaa-r, 5′- CCCAAGAGCCATCCA CGAT -3′; pappab-f 5′-ATACGCGTCTTGACAGGCTT-3′; pappab-r, 5′- TAAGCAAACCAAACCTCCGA-3′; pappa2-f, 5′-CTTGTCGGTTGTTTCTGCTT-3′; pappa2-r, 5′-CTTCTTTTCAGCTCGCATTT-3′.

Cartilage staining

Staining with Alcian blue was performed using a previously published protocol[59] with minor adaptions. Larvae were euthanized and fixed in 4% PFA in PBS (pH 7.4) for 72 h at 4 °C. After 3 × 5 min washing in PBT (PBS pH 7.4, 0.01% Tween), the larvae were bleached in 3% H_2O_2/1% KOH in PBS (pH 7.4). This was followed by 3 × 5 min of washing in PBS (pH 7.4), after which the larvae were transferred to Alcian blue staining solution (0.02% Alcian blue 8GX (Sigma Aldrich) dissolved in 80% EtOH/20% glacial acetic acid) and incubated overnight at 4°C with gentle agitation. Subsequently, the larvae were destained in 70% EtOH/5% HCl with consecutive changes of destain solution. The larvae were gradually rehydrated into PBT (PBS pH 7.4, 0.01% Tween) and cleared in 0.05% trypsin in PBT overnight at 4°C. The specimens were then re-fixed in 4% PFA for 2 h at RT before transfer to 100% glycerol. In Alcian blue-stained specimens, the length of Meckel's cartilage was determined as the distance from the anterior most part of the element to the posterior edge of the element, where it articulates with the palatoquadrate cartilage. All measurements were performed using ImageJ.

Whole mount in situ hybridization

After euthanasia, the larvae were fixated in 4% PFA overnight at 4°C. This was followed by bleaching in 3%H_2O_2/0.5% KOH to reduce head pigmentation. The specimens were then dehydrated in gradually increasing amounts of MeOH in PBS (adjusted to pH 5.5) and kept in 100% MeOH for minimum 2 h at -20°C. The procedure was performed according to Thisse et al.[60], with the addition of 5% (w/v) dextran sulfate (Mr > 500,000 Sigma) to the hybridization mix to improve the signal-to-noise ratio. Gene specific probes were generated using the following primers: *sox9a-f*: 5′- AAAAGCGAGCACCGTGGATTTG-3′, *sox9a-r*: 5′- GACGCTTTT CCACCTCGTTCAGTA- 3′; *ihha-f*: 5′- AGTGGAGGCCGGTTTTGATT-3′, *ihha-r*: 5′- TCGAGCACTTGAGTT CCGAT-3′; *col10a1a-f*: 5′- AGGTCATACAGGTGCTACTGGT-3′, *col10a1a-r*: 5′- AGCACAGTCTGTTGTGCA TCAT -3′; *pappaa*-f: 5′-GGCCAACAAGCCAAAGAGGAG-3′, *pappaa*-r: 5′-GCTGGTGGTCATGTTACCCG-3. The intensities of the differentiation markers *sox9a*, *ihha,* and *col10a1a* were quantified using ImageJ. On ventral images, regions capturing each of the bilateral parts of Meckel's cartilage (*sox9a* and *col10a1a*), or the ceratohyal cartilage (*ihha*) were selected and background subtracted by rolling average. Measured intensities of the bilateral elements were averaged.

Pharmacological treatments

Larvae were treated with the compounds: BMS-754807 (Selleck Chemicals)[29] and NVP-AEW541[30] (Cayman Chemical). Both compounds were dissolved in 100% DMSO and dilutions made in E3 buffer. BMS-754807 was administered in a final concentration of 0.45 µM, whereas NVP-AEW541 was used in a final concentration of 4 µM. For both treatments, the larvae (AB wild-type) were raised in the drug solution for 24 h from 3 to 4 dpf, after which they were euthanized and Alcian blue-stained. Different doses of the two compounds were

prescreened for potential effects on larval health, gross behavior and morphology. For rescue experiments, human recombinant IGF-I (GroPep) was added to the E3 buffer to a final concentration of 30 ng/mL[57].

Imaging of zebrafish

Images of whole mount-unstained zebrafish larvae, Alcian blue-stained specimens, and in situ-stained zebrafish larvae were captured using an Olympus IX71 microscope equipped with an Olympus DP71 camera. A Photonic LED light source was used for imaging of in situ-stained larvae. Whole mount unstained larvae were mounted in 4% methylcellulose for imaging, stained specimens were mounted in 100% glycerol. Confocal images were captured using a Zeiss AxioImager.Z2 confocal microscope equipped with an LSM 780 unit and an Axiocam-MRm camera. The larvae were sedated in 150 mg/L buffered Tricaine for 10 min and mounted in 1% low melt agarose. The embedded larvae were then covered with buffered Tricaine and z-stack images captured. Cell length and width was measured for the chondrocytes making up the middle third of Meckel's cartilage. For each chondrocyte, the number of neighboring cells to which a cell makes direct contact was also determined.

Statistical analysis

Statistical analysis was performed using GraphPad Prism 7. Specific statistical tests used are specified in the relevant paragraphs. Data is presented as mean ± SD unless otherwise stated.

Data availability

The datasets used and/or analyzed during the current study available from the corresponding author on reasonable request.

Received: 15 July 2024; Accepted: 23 August 2024
Published online: 29 August 2024

References

1. Yakar, S. & Isaksson, O. Regulation of skeletal growth and mineral acquisition by the GH/IGF-1 axis: Lessons from mouse models. *Growth Horm. IGF Res.* **28**, 26–42. https://doi.org/10.1016/j.ghir.2015.09.004 (2016).
2. Oxvig, C. & Conover, C. A. The Stanniocalcin-PAPP-A-IGFBP-IGF Axis. *J. Clin Endocrinol. Metab.* https://doi.org/10.1210/clinem/dgad053 (2023).
3. Racine, H. L. & Serrat, M. A. The actions of IGF-1 in the growth plate and its role in postnatal bone elongation. *Curr. Osteoporos. Rep.* **18**, 210–227. https://doi.org/10.1007/s11914-020-00570-x (2020).
4. Kronenberg, H. M. Developmental regulation of the growth plate. *Nature* **423**, 332–336. https://doi.org/10.1038/nature01657 (2003).
5. Dixit, M., Poudel, S. B. & Yakar, S. Effects of GH/IGF axis on bone and cartilage. *Mol. Cell Endocrinol.* **519**, 111052. https://doi.org/10.1016/j.mce.2020.111052 (2021).
6. Mushtaq, T., Bijman, P., Ahmed, S. F. & Farquharson, C. Insulin-like growth factor-I augments chondrocyte hypertrophy and reverses glucocorticoid-mediated growth retardation in fetal mice metatarsal cultures. *Endocrinology* **145**, 2478–2486. https://doi.org/10.1210/en.2003-1435 (2004).
7. Forbes, B. E., McCarthy, P. & Norton, R. S. Insulin-like growth factor binding proteins: A structural perspective. *Front. Endocrinol. (Lausanne)* **3**, 38. https://doi.org/10.3389/fendo.2012.00038 (2012).
8. Oxvig, C. The role of PAPP-A in the IGF system: Location, location, location. *J. Cell Commun. Signal* **9**, 177–187. https://doi.org/10.1007/s12079-015-0259-9 (2015).
9. Argente, J., Chowen, J. A., Perez-Jurado, L. A., Frystyk, J. & Oxvig, C. One level up: Abnormal proteolytic regulation of IGF activity plays a role in human pathophysiology. *EMBO Mol. Med.* **9**, 1338–1345. https://doi.org/10.15252/emmm.201707950 (2017).
10. Kobbero, S. D. *et al.* Structure of the proteolytic enzyme PAPP-A with the endogenous inhibitor stanniocalcin-2 reveals its inhibitory mechanism. *Nat. Commun.* **13**, 6084. https://doi.org/10.1038/s41467-022-33698-8 (2022).
11. Conover, C. A. & Oxvig, C. The pregnancy-associated plasma protein-A (PAPP-A) story. *Endocr. Rev.* https://doi.org/10.1210/endrev/bnad017 (2023).
12. Monget, P. *et al.* Pregnancy-associated plasma protein-A is involved in insulin-like growth factor binding protein-2 (IGFBP-2) proteolytic degradation in bovine and porcine preovulatory follicles: identification of cleavage site and characterization of IGFBP-2 degradation. *Biol. Reprod.* **68**, 77–86. https://doi.org/10.1095/biolreprod.102.007609 (2003).
13. Lawrence, J. B. *et al.* The insulin-like growth factor (IGF)-dependent IGF binding protein-4 protease secreted by human fibroblasts is pregnancy-associated plasma protein-A. *Proc. Natl. Acad. Sci. USA* **96**, 3149–3153. https://doi.org/10.1073/pnas.96.6.3149 (1999).
14. Laursen, L. S. *et al.* Pregnancy-associated plasma protein-A (PAPP-A) cleaves insulin-like growth factor binding protein (IGFBP)-5 independent of IGF: Implications for the mechanism of IGFBP-4 proteolysis by PAPP-A. *FEBS Lett* **504**, 36–40. https://doi.org/10.1016/s0014-5793(01)02760-0 (2001).
15. Conover, C. A. *et al.* Metalloproteinase pregnancy-associated plasma protein A is a critical growth regulatory factor during fetal development. *Development* **131**, 1187–1194. https://doi.org/10.1242/dev.00997 (2004).
16. Tanner, S. J., Hefferan, T. E., Rosen, C. J. & Conover, C. A. Impact of pregnancy-associated plasma protein-a deletion on the adult murine skeleton. *J. Bone Miner. Res.* **23**, 655–662. https://doi.org/10.1359/jbmr.071210 (2008).
17. Mork, L. & Crump, G. Zebrafish craniofacial development: a window into early patterning. *Curr. Top. Dev. Biol.* **115**, 235–269. https://doi.org/10.1016/bs.ctdb.2015.07.001 (2015).
18. Ling, I. T., Rochard, L. & Liao, E. C. Distinct requirements of wls, wnt9a, wnt5b and gpc4 in regulating chondrocyte maturation and timing of endochondral ossification. *Dev. Biol.* **421**, 219–232. https://doi.org/10.1016/j.ydbio.2016.11.016 (2017).
19. Kjaer-Sorensen, K. *et al.* Pregnancy-associated plasma protein A (PAPP-A) modulates the early developmental rate in zebrafish independently of its proteolytic activity. *J. Biol. Chem.* **288**, 9982–9992. https://doi.org/10.1074/jbc.M112.426304 (2013).
20. Gyrup, C. & Oxvig, C. Quantitative analysis of insulin-like growth factor-modulated proteolysis of insulin-like growth factor binding protein-4 and -5 by pregnancy-associated plasma protein-A. *Biochemistry* **46**, 1972–1980. https://doi.org/10.1021/bi062229i (2007).
21. Boldt, H. B. *et al.* The Lin12-notch repeats of pregnancy-associated plasma protein-A bind calcium and determine its proteolytic specificity. *J. Biol. Chem.* **279**, 38525–38531. https://doi.org/10.1074/jbc.M405222200 (2004).
22. Soe, R. *et al.* Expression of recombinant murine pregnancy-associated plasma protein-A (PAPP-A) and a novel variant (PAPP-Ai) with differential proteolytic activity. *Eur. J. Biochem.* **269**, 2247–2256. https://doi.org/10.1046/j.1432-1033.2002.02883.x (2002).

23. Schilling, T. F. *et al.* Jaw and branchial arch mutants in zebrafish I: Branchial arches. *Development* **123**, 329–344. https://doi.org/10.1242/dev.123.1.329 (1996).
24. Le Pabic, P., Ng, C. & Schilling, T. F. Fat-Dachsous signaling coordinates cartilage differentiation and polarity during craniofacial development. *PLoS Genet* **10**, e1004726. https://doi.org/10.1371/journal.pgen.1004726 (2014).
25. Lawson, N. D. & Weinstein, B. M. In vivo imaging of embryonic vascular development using transgenic zebrafish. *Dev. Biol.* **248**, 307–318. https://doi.org/10.1006/dbio.2002.0711 (2002).
26. Bi, W., Deng, J. M., Zhang, Z., Behringer, R. R. & De Crombrugghe, B. Sox9 is required for cartilage formation. *Nat. Genetics* **22**, 85–89 (1999).
27. St-Jacques, B., Hammerschmidt, M. & McMahon, A. P. Indian hedgehog signaling regulates proliferation and differentiation of chondrocytes and is essential for bone formation. *Genes Dev.* **13**, 2072–2086 (1999).
28. Eames, B. F., Amores, A., Yan, Y. L. & Postlethwait, J. H. Evolution of the osteoblast: Skeletogenesis in gar and zebrafish. *BMC Evolut. Biol. 12* (2012).
29. Garcia-Echeverria, C. *et al.* In vivo antitumor activity of NVP-AEW541-A novel, potent, and selective inhibitor of the IGF-IR kinase. *Cancer Cell* **5**, 231–239 (2004).
30. Awasthi, N., Zhang, C., Ruan, W., Schwarz, M. A. & Schwarz, R. E. BMS-754807, a small-molecule inhibitor of insulin-like growth factor-1 receptor/insulin receptor, enhances gemcitabine response in pancreatic cancer. *Mol. Cancer Ther.* **11**, 2644–2653. https://doi.org/10.1158/1535-7163.MCT-12-0447 (2012).
31. Guevara-Morales, J. M. *et al.* Growth plate pathology in the mucopolysaccharidosis type vi rat model-an experimental and computational approach. *Diagnostics (Basel)*. https://doi.org/10.3390/diagnostics10060360 (2020).
32. Wang, Y. *et al.* IGF-1R signaling in chondrocytes modulates growth plate development by interacting with the PTHrP/Ihh pathway. *J. Bone Miner. Res.* **26**, 1437–1446. https://doi.org/10.1002/jbmr.359 (2011).
33. Wang, J., Zhou, J. & Bondy, C. A. Igf1 promotes longitudinal bone growth by insulin-like actions augmenting chondrocyte hypertrophy. *FASEB J.* **13**, 1985–1990. https://doi.org/10.1096/fasebj.13.14.1985 (1999).
34. Dauber, A. *et al.* Mutations in pregnancy-associated plasma protein A2 cause short stature due to low IGF-I availability. *EMBO Mol. Med.* **8**, 363–374. https://doi.org/10.15252/emmm.201506106 (2016).
35. Laursen, L. S. *et al.* Cell surface targeting of pregnancy-associated plasma protein A proteolytic activity. Reversible adhesion is mediated by two neighboring short consensus repeats. *J. Biol. Chem.* **277**, 47225–47234. https://doi.org/10.1074/jbc.M209155200 (2002).
36. Laursen, L. S., Kjaer-Sorensen, K., Andersen, M. H. & Oxvig, C. Regulation of insulin-like growth factor (IGF) bioactivity by sequential proteolytic cleavage of IGF binding protein-4 and -5. *Mol. Endocrinol.* **21**, 1246–1257. https://doi.org/10.1210/me.2006-0522 (2007).
37. Lloyd, K. A. *et al.* Netazepide inhibits expression of pappalysin 2 in type 1 gastric neuroendocrine tumors. *Cell. Mol. Gastroenterol. Hepatol.* **10**, 113–132. https://doi.org/10.1016/j.jcmgh.2020.01.010 (2020).
38. Sjogren, K. *et al.* Liver-derived insulin-like growth factor I (IGF-I) is the principal source of IGF-I in blood but is not required for postnatal body growth in mice. *Proc. Natl. Acad. Sci. USA* **96**, 7088–7092. https://doi.org/10.1073/pnas.96.12.7088 (1999).
39. Yakar, S. *et al.* Normal growth and development in the absence of hepatic insulin-like growth factor I. *Proc. Natl. Acad. Sci. USA* **96**, 7324–7329. https://doi.org/10.1073/pnas.96.13.7324 (1999).
40. Jepsen, M. R. *et al.* Stanniocalcin-2 inhibits mammalian growth by proteolytic inhibition of the insulin-like growth factor axis. *J. Biol. Chem.* **290**, 3430–3439. https://doi.org/10.1074/jbc.M114.611665 (2015).
41. Ohlsson, C. *et al.* The role of liver-derived insulin-like growth factor-I. *Endocr Rev* **30**, 494–535. https://doi.org/10.1210/er.2009-0010 (2009).
42. Marchant, C., Anderson, P., Schwarz, Q. & Wiszniak, S. Vessel-derived angiocrine IGF1 promotes Meckel's cartilage proliferation to drive jaw growth during embryogenesis. *Development* https://doi.org/10.1242/dev.190488 (2020).
43. Parker, E. A. *et al.* Spatial and temporal regulation of GH-IGF-related gene expression in growth plate cartilage. *J. Endocrinol.* **194**, 31–40. https://doi.org/10.1677/JOE-07-0012 (2007).
44. Kiepe, D., Ciarmatori, S., Haarmann, A. & Tonshoff, B. Differential expression of IGF system components in proliferating vs. differentiating growth plate chondrocytes: The functional role of IGFBP-5. *Am. J. Physiol. Endocrinol. Metab.* **290**, E363-371. https://doi.org/10.1152/ajpendo.00363.2005 (2006).
45. Marouli, E. *et al.* Rare and low-frequency coding variants alter human adult height. *Nature* **542**, 186–190. https://doi.org/10.1038/nature21039 (2017).
46. Glerup, S. *et al.* Cell surface detachment of pregnancy-associated plasma protein-A requires the formation of intermolecular proteinase-inhibitor disulfide bonds and glycosaminoglycan covalently bound to the inhibitor. *J. Biol. Chem.* **282**, 1769–1778. https://doi.org/10.1074/jbc.M608454200 (2007).
47. Kloverpris, S. *et al.* Stanniocalcin-1 potently inhibits the proteolytic activity of the metalloproteinase pregnancy-associated plasma protein-A. *J. Biol. Chem.* **290**, 21915–21924. https://doi.org/10.1074/jbc.M115.650143 (2015).
48. Bittner, N. *et al.* Primary osteoarthritis chondrocyte map of chromatin conformation reveals novel candidate effector genes. *Ann. Rheum. Dis.* https://doi.org/10.1136/ard-2023-224945 (2024).
49. Concordet, J. P. & Haeussler, M. CRISPOR: Intuitive guide selection for CRISPR/Cas9 genome editing experiments and screens. *Nucleic Acids Res.* **46**, W242–W245. https://doi.org/10.1093/nar/gky354 (2018).
50. Ran, F. A. *et al.* Genome engineering using the CRISPR-Cas9 system. *Nat. Protoc* **8**, 2281–2308. https://doi.org/10.1038/nprot.2013.143 (2013).
51. Swiatek, P. J. & Gridley, T. Perinatal lethality and defects in hindbrain development in mice homozygous for a targeted mutation of the zinc finger gene Krox20. *Genes Dev.* **7**, 2071–2084. https://doi.org/10.1101/gad.7.11.2071 (1993).
52. Brinkman, E. K., Chen, T., Amendola, M. & van Steensel, B. Easy quantitative assessment of genome editing by sequence trace decomposition. *Nucleic Acids Res.* **42**, e168. https://doi.org/10.1093/nar/gku936 (2014).
53. Wertz, K. & Fuchtbauer, E. M. Dmd(mdx-beta geo): A new allele for the mouse dystrophin gene. *Dev. Dyn.* **212**, 229–241. https://doi.org/10.1002/(SICI)1097-0177(199806)212:2%3c229::AID-AJA7%3e3.0.CO;2-J (1998).
54. Boldt, H. B., Glerup, S., Overgaard, M. T., Sottrup-Jensen, L. & Oxvig, C. Definition, expression, and characterization of a protein domain in the N-terminus of pregnancy-associated plasma protein-A distantly related to the family of laminin G-like modules. *Protein Expr. Purif.* **48**, 261–273. https://doi.org/10.1016/j.pep.2006.01.024 (2006).
55. Schneider, C. A., Rasband, W. S. & Eliceiri, K. W. NIH Image to ImageJ: 25 years of image analysis. *Nat. Methods* **9**, 671–675. https://doi.org/10.1038/nmeth.2089 (2012).
56. Kettleborough, R. N. *et al.* A systematic genome-wide analysis of zebrafish protein-coding gene function. *Nature* **496**, 494–497. https://doi.org/10.1038/nature11992 (2013).
57. Liu, C. *et al.* The metalloproteinase Papp-aa controls epithelial cell quiescence-proliferation transition. *Elife.* https://doi.org/10.7554/eLife.52322 (2020).
58. Breacker, C., Barber, I., Norton, W. H., McDearmid, J. R. & Tilley, C. A. A low-cost method of skin swabbing for the collection of DNA samples from small laboratory fish. *Zebrafish* **14**, 35–41. https://doi.org/10.1089/zeb.2016.1348 (2017).
59. Neuhauss, S. F. C. *et al.* Mutations affecting craniofacial development in zebrafish. *Development* **123**, 357–367 (1996).
60. Thisse, C. & Thisse, B. High-resolution in situ hybridization to whole-mount zebrafish embryos. *Nat. Protocols* **3**, 59–69. https://doi.org/10.1038/nprot.2007.514 (2008).

Acknowledgements
The technical support of Jytte Utoft and Inger-Merete Paulsen is gratefully acknowledged. This research was supported by grants to C.O. from the Independent Research Fund Denmark, the Carlsberg Foundation, and the Novo Nordisk Foundation.

Author contributions
M.H., K.K.S., and C.O. designed the study; E.M.F. helped with the generation of genetically modified mice; J.S.T., A.B., and R.A.F. helped with the analysis of murine tissues; M.H. and C.O. drafted the manuscript. All authors reviewed and approved the final version.

Competing interests
The authors declare no competing interests.

Additional information
Correspondence and requests for materials should be addressed to C.O.

Reprints and permissions information is available at www.nature.com/reprints.

Publisher's note Springer Nature remains neutral with regard to jurisdictional claims in published maps and institutional affiliations.